Volume 48 | Number 29 | 7 August 2019 | Pages 10757–11146

Dalton Transactions

An international journal of inorganic chemistry

rsc.li/dalton

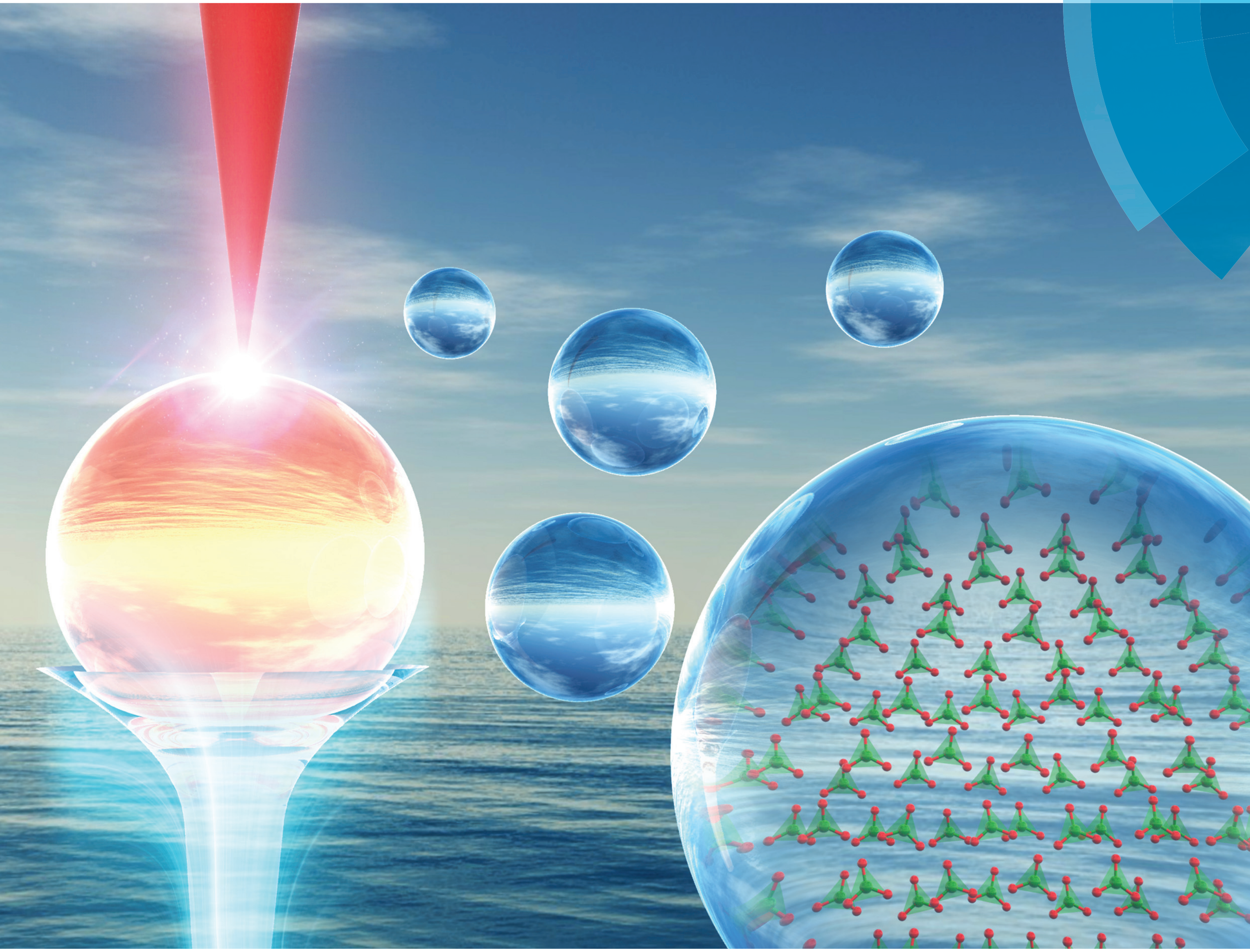

ISSN 1477-9226

ROYAL SOCIETY OF CHEMISTRY | Celebrating IYPT 2019

PAPER

Atsunobu Masuno *et al.*

High refractive index La-rich lanthanum borate glasses composed of isolated BO_3 units

Dalton Transactions

PAPER

View Article Online
View Journal | View Issue

Cite this: *Dalton Trans.*, 2019, **48**, 10804

High refractive index La-rich lanthanum borate glasses composed of isolated BO_3 units

Atsunobu Masuno, *[a,b,c] Takashi Iwata,[d] Yutaka Yanaba,[b] Shunta Sasaki,[a] Hiroyuki Inoue[b] and Yasuhiro Watanabe[b]

Received 24th April 2019,
Accepted 7th June 2019

DOI: 10.1039/c9dt01715a

rsc.li/dalton

La_2O_3–B_2O_3 binary glasses were prepared by containerless processing using a levitation technique. The bulk glass-forming region in a B-rich composition was extended compared to that using conventional melt-quench techniques. Furthermore, additional glass formation was realized in an La-rich composition. The glass transition temperature and crystallization temperature of La-rich glasses are much higher than those of B-rich glasses. Both B- and La-rich glasses were colorless and transparent and had a high refractive index with low wavelength dispersion in the visible region. With the increase of the La_2O_3 content, the optical absorption edge in the ultraviolet (UV) region shifts to a long wavelength. An additional infrared (IR) transmittance window was observed in La-rich glasses, indicating that the La-rich borate glasses are expected to be used in optical components in a wide wavelength region. Local structural analyses using ^{11}B magic-angle spinning (MAS) nuclear magnetic resonance (NMR) and Raman scattering spectra revealed that every B-atom in La-rich glasses formed a planar trigonal BO_3 unit and these BO_3 units were entirely isolated. The evident difference from B-rich glasses where B-atoms formed a complex network structure with BO_3 and BO_4 units caused the characteristic physical and optical properties of La-rich glasses.

Introduction

Containerless processing is a way to keep a material in the air by a levitation technique using some types of force to resist gravity, such as electromagnetic force, electrostatic force, magnetic force, sound waves, and gas flow.[1] By applying laser heating, the material can be melted while being levitated. Because no container, such as a crucible, is used to hold the melt, containerless processing can suppress heterogeneous nucleation that occurs at the boundary between the melt and the container's wall. Deep undercooling of the melt can thus be promoted,[2] which often leads to glass formation without crystallization even if the material has a low glass-forming ability. Accordingly, this process employing levitation has been recognized as an approach not only to extend the glass-forming region of conventional oxide glasses,[3,4] but also to develop new glass systems.[5–10]

Among new glasses obtained by containerless processing, some binary oxide systems without any network former oxides have characteristic optical properties. TiO_2-,[11] Nb_2O_5-,[12] WO_3-,[8] and Ga_2O_3-based[13] binary glasses are colorless and transparent and have a high refractive index (n_d) over 1.9 to 2.35 at 587.65 nm. It should be noted that these glasses show low wavelength dispersion. Using high refractive index glass with low wavelength dispersion as a lens, focal points for various wavelengths get close in a wide wavelength region. Chromatic aberration is thus suppressed. Therefore, a high refractive index and low wavelength dispersion are the desired properties in the field of optical glasses. In order to improve optical properties regarding the refractive index, various third components were added to TiO_2-, Nb_2O_5-, and Ga_2O_3-based glasses. Some glasses having a high refractive index with low wavelength dispersion were successfully obtained.[14–17] Although the third components were effective in reducing the wavelength dispersion, the refractive index still decreased in the cases of high refractive index TiO_2-, Nb_2O_5-, and Ga_2O_3-based glasses. Therefore, previous studies whose aim was to develop high refractive index glasses with low wavelength dispersion were oriented toward decreasing the wavelength dispersion and keeping the refractive index high.

Besides the aim of obtaining high refractive index glasses with low wavelength dispersion as mentioned above, there must be an opposite approach to increase the refractive index

---

[a] *Graduate School of Science and Technology, Hirosaki University, 3 Bunkyo-cho, Hirosaki, Aomori 036-8561, Japan. E-mail: masuno@hirosaki-u.ac.jp*

[b] *Institute of Industrial Science, The University of Tokyo, 4-6-1 Komaba, Meguro-ku, Tokyo 153-8505, Japan*

[c] *Center for Materials Research by Information Integration, Research and Services Division of Materials Data and Integrated System, National Institute for Materials Science, 1-2-1 Sengen, Tsukuba, Ibaraki 305-0047, Japan*

[d] *Shibaura Institute of Technology, 3-7-5 Toyosu, Koto-ku, Tokyo 135-8548, Japan*

of low wavelength dispersion glasses. It is well known that commercial optical glasses with low wavelength dispersion and a comparatively high refractive index (n_d = 1.7–1.8) are designed on the basis of rare-earth borate composition.[18,19] It was reported that La_2O_3–B_2O_3 binary glasses were formed in the range 0–28 mol% La_2O_3 by the conventional melt-quench technique. However, glasses with 2–22 mol% La_2O_3 were milky and phase-separated owing to the immiscibility of the liquids.[20,21] Therefore, the content of La_2O_3 required to obtain clear and homogeneous glasses is limited in the vicinity of 25 mol%.[20–27] Nevertheless, if La_2O_3 content of the glasses increases, the refractive index of the glasses with low wavelength dispersion will increase because La_2O_3 is regarded as a key component to increase the refractive index, besides TiO_2 and Nb_2O_5. In this study, containerless processing was applied to La_2O_3–B_2O_3 glasses in order to obtain high-La_2O_3-content glasses. Glass formation in La_2O_3-rich compositions in La_2O_3–B_2O_3 binary systems is reported. In addition, the thermal, optical, and structural properties of the glasses were investigated.

Experimental procedures

High-purity La_2O_3 and H_3BO_3 powders were mixed stoichiometrically in the composition of $x La_2O_3$–$(100 - x)B_2O_3$. The mixtures were pelletized and sintered at 600 °C for 12 h to remove H_2O. A piece of ~20 mg was taken from the crushed pellets as a target and placed on the nozzle of an aerodynamic levitation furnace and levitated by O_2 gas, with the flow rate controlled by a mass-flow controller. A 100 W CO_2 laser was used to melt the levitated target. The temperature was monitored using a pyrometer with a 100 Hz sampling rate. The melt was maintained above its melting point for a few seconds in order to achieve homogeneity. The laser power was set as low as possible to avoid evaporation of the target. Then, the laser was turned off, and the melt was cooled naturally down to room temperature at the rate of several hundred kelvins per second. The solidified samples were spherical, and their diameters were approximately 2–3 mm.

Cu Kα X-ray diffraction (XRD) patterns were measured to confirm glass formation. Inductively coupled plasma atomic emission spectrometry (ICP-AES) analysis indicated the composition deviation of some glasses from the target material was less than approximately 3 mol%. A differential thermal analysis (DTA) at a heating rate of 10 °C min^{-1} was performed to determine the glass transition temperature (T_g) and the crystallization on-set temperature (T_x) (SII, TG/DTA6300). All the glasses were annealed slightly above T_g for 10 min to remove internal strain before physical property measurements. The densities of glasses were measured on a gas pycnometer (AccuPycII 1340; Micromeritics). For the transmittance measurement, both sides of the glass samples were optically polished to a thickness of ~500 μm. The transmittance spectra were measured using an ultraviolet–visible (UV-Vis) spectrometer (UV3100PC; Shimadzu) in the range of 250–2000 nm and using a Fourier transform infrared spectrometer (FTIR 8200; Shimadzu) in the range of 2000–10 000 nm. In order to measure the refractive index, a spectroscopic ellipsometer (M-2000F; J.A. Woollam) was used in the range of 250–1000 nm. The incident light was at an angle of 75° to the glass surface.

Unpolarized Raman scattering spectra were obtained in a 180° scattering geometry on a T-64000 Jobin–Yvon spectrometer equipped with a liquid-nitrogen-cooled CCD detector. The incident source was an Ar^+ ion laser of 514.5 nm operating at 250 mW. ^{11}B nuclear magnetic resonance (NMR) spectroscopy measurements were performed on a JEOL JNM-ECA 500 spectrometer at 11.74 T (^1H-500 MHz) equipped with a magic-angle spinning (MAS) probe head (spinning rate: 15 kHz, zirconia rotor of a 4 mm diameter). The NMR spectra were recorded using $\mu/6$ pulses (1.0 μs) and a relaxation delay of 30 s and 64 accumulated signal transients. ^{11}B chemical shifts are expressed in parts per million (ppm) relative to 1 M boric acid at 19.5 ppm. The decomposition of the NMR spectra was performed using the "dmfit" program.[28] All of the measurements except for the DTA were performed at room temperature.

Results and discussion

Glass-forming region

Fig. 1 is a phase diagram of the La_2O_3–B_2O_3 binary system[21] together with glass-forming regions. The glass-forming region was reported to be limited in a very narrow region in B-rich compositions around $22 \le x \le 28$ in bulk form by the conventional melt-quench method and up to x = 30 in flake form by the twin roller rapid quench technique.[20,26] The bulk glass-forming region was expanded to x = 35 using the levitation

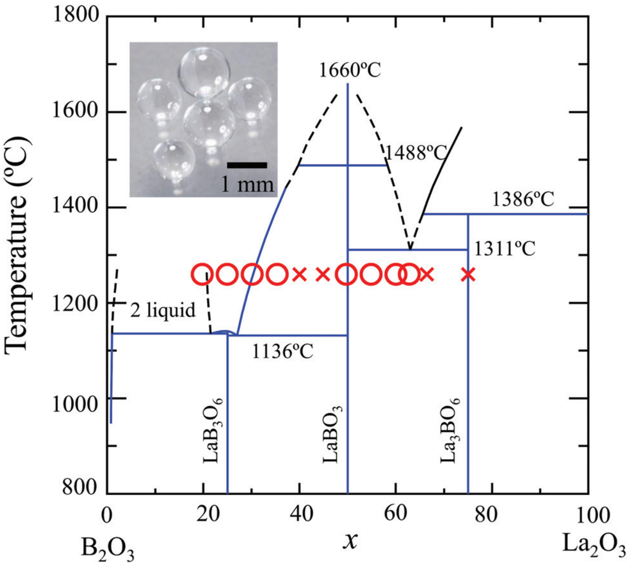

Fig. 1 Glass-forming regions on the phase diagram of the La_2O_3–B_2O_3 binary system.[21] The open and cross symbols represent glass formation and crystallization, respectively. The inset is a picture of the glasses obtained.

technique. Furthermore, glass formations were found in not only the B-rich composition range, but also the La-rich composition range. The newly discovered La-rich glass-forming region was $50 \leq x \leq 63$. The edges of the glass-forming region correspond to the crystalline phase $LaBO_3$ ($x = 50$), and the eutectic point was at $x = 63$. No glass formation was observed in other compositions. The liquid state of this region is thus peculiarly easy to amorphasize differently from others. The occurrence of two separate glass-forming regions is of particular note, because there are very few reports on more than one glass-forming region in binary oxide systems such as the Na_2O–B_2O_3 system and the La_2O_3–Nb_2O_5 system.[29,30] As reported in La_2O_3–Nb_2O_5 glasses, the structures of B- and La-rich glasses might have different connectivity. In both regions of B- and La-rich compositions, colorless and transparent sphere glasses were obtained as shown in the inset.

Physical properties

The composition dependences of the glass transition temperature (T_g) and the crystallization on-set temperature (T_x) of xLa$_2$O$_3$–(100 − x)B$_2$O$_3$ glasses are shown in Fig. 2(a). Both T_g and T_x decreased by increasing the La_2O_3 content in B- and La-rich glasses. However, it is clearly seen that both T_g and T_x of La-rich glasses are much higher than those of B-rich glasses. The obvious difference in the temperature region between B- and La-rich glasses suggests a difference in the glassy state itself, which might be one of evidences of the connectivity change from B-rich glasses to La-rich glasses. The temperature difference between T_g and T_x ($\Delta T = T_x - T_g$) is a measure of glass stability against crystallization. ΔT was decreased by increasing the La_2O_3 content, as shown in Fig. 2(b). However, although ΔT of La-rich glasses was small, its glass formation is easy comparable to B-rich glasses. The melting point of the glasses has not been determined in this study because of the measurement limit for especially La-rich glasses. Nevertheless, the observation at the levitation experiments indicated the melting point of the glasses seemed to be close to the liquidus temperature shown on the phase diagram of La_2O_3–B_2O_3 binary system.

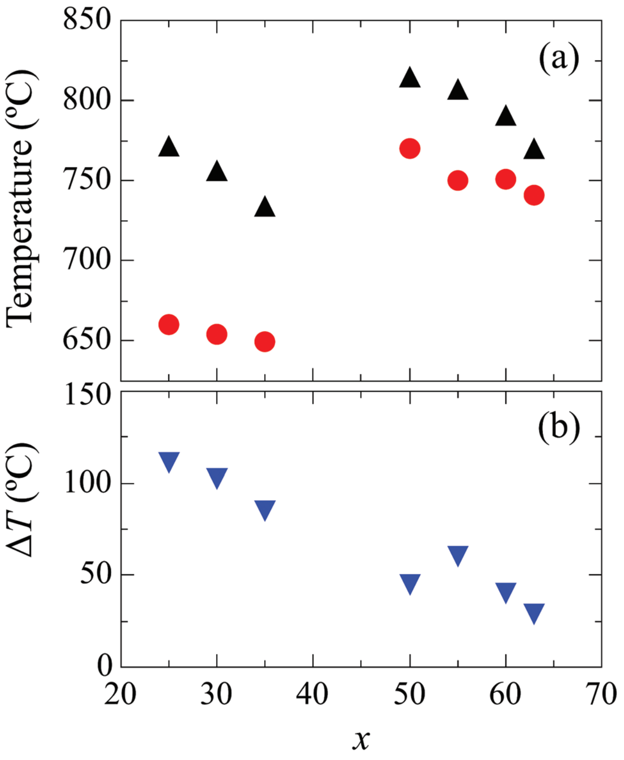

Fig. 2 (a) Glass transition temperature (T_g) (red circles) and crystallization on-set temperature (T_x) (black triangles). (b) $\Delta T = T_x - T_g$ of xLa$_2$O$_3$–(100 − x)B$_2$O$_3$ glasses.

Fig. 3 shows the density of xLa$_2$O$_3$–(100 − x)B$_2$O$_3$ glasses together with the values from references.[20] There is no reliable data in the vicinity of $x = 10$ because the region corresponds to the phase separation region. Nevertheless, the density in the B-rich region increased linearly. It is clearly seen that the density increased monotonically with x. However, the increase in the slope became more gentle in the La-rich region.

Fig. 4 shows the transmittance spectra of xLa$_2$O$_3$–(100 − x)B$_2$O$_3$ glasses in the UV-Vis region. The absorption edge of the $x = 25$ glass was approximately 200 nm. The absorption edge shifted toward long wavelengths by increasing the La_2O_3 content. At the highest La_2O_3 composition of $x = 63$, the absorption edge was still below 250 nm, indicating that the glasses are good transparent media in the UV-Vis region. The optical band gap energy (E_g) was estimated from the wavelength of the absorption edge.[11] E_g was decreased monotonically from 6.2 to 5.1 eV by increasing the La_2O_3 content, as shown in the inset. The valence band is originated from O 2p band, while the conduction band is from cation band.

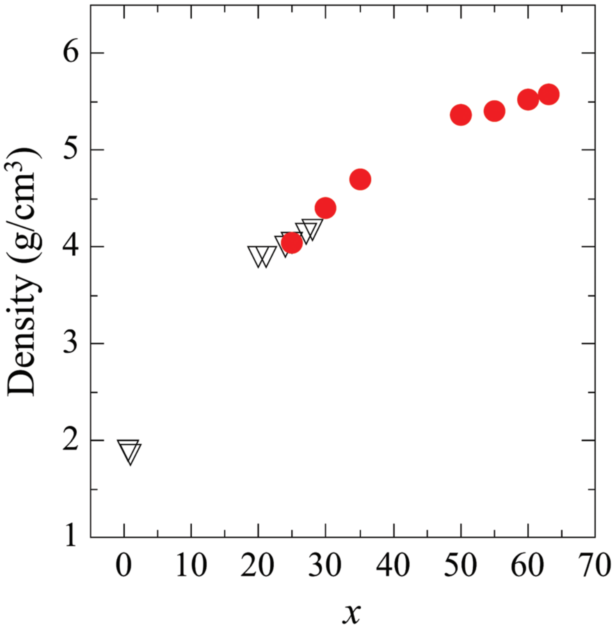

Fig. 3 Densities of xLa$_2$O$_3$–(100 − x)B$_2$O$_3$ glasses. The closed circles represent the data obtained in this study. The open symbols represent data from a reference.[20]

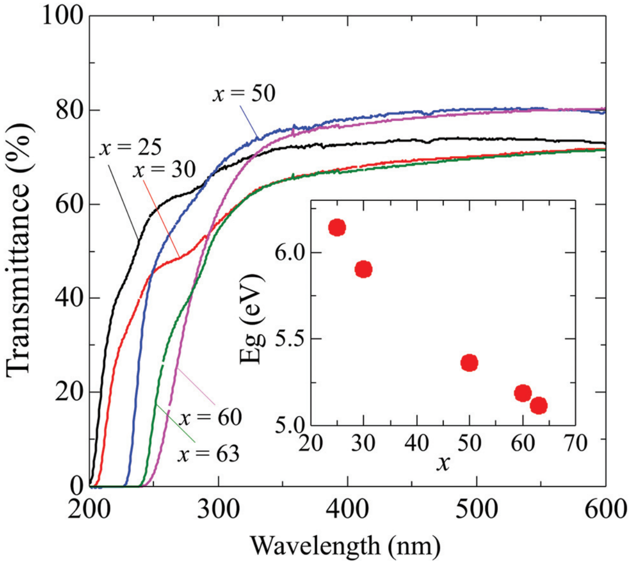

Fig. 4 Transmittance spectra in the UV-Vis region of $x\mathrm{La_2O_3}$–(100 − x)$\mathrm{B_2O_3}$ glasses. The inset shows the composition dependence of the optical bandgap (E_g).

Decreasing E_g by adding $\mathrm{La_2O_3}$ to the system means that the conduction band originated from $\mathrm{La^{3+}}$ developed to the lower energy side compared to that of $\mathrm{B^{3+}}$. Accordingly, the band gap was dominated by the density of state of La and O. Below 300 nm, there were some small absorption bands that were likely to be assigned to the absorption by O–H bonds in the glasses. These bands can be eliminated by careful optimization of the melting process and the removal of the water content in raw materials.

The infrared (IR) transmittance spectra of $x\mathrm{La_2O_3}$–(100 − x)$\mathrm{B_2O_3}$ glasses are shown in Fig. 5. It is clearly seen that the main absorption edge was approximately 2700 $\mathrm{cm^{-1}}$ (3.7 μm) of the x = 25 glass, and there were small transmittance windows at 2500 $\mathrm{cm^{-1}}$ (4.0 μm) and 2000 $\mathrm{cm^{-1}}$ (5.0 μm). At x = 30, the main absorption edge shifted toward the long wavelength side. Furthermore, the peaks of the two small transmittance windows also shifted toward the long wavelength side at 2435 $\mathrm{cm^{-1}}$ (4.1 μm) and 1910 $\mathrm{cm^{-1}}$ (5.2 μm), and the transmittance increased. In the La-rich region, two transmittance windows at approximately 2300 $\mathrm{cm^{-1}}$ (4.3 μm) and 1800 $\mathrm{cm^{-1}}$ (5.6 μm) were clearly observed. The peak of the 2300 $\mathrm{cm^{-1}}$ band shifted toward the long wavelength side by increasing x, whereas the peaks of the 1800 $\mathrm{cm^{-1}}$ band did not shift. It is unclear whether the two obvious transmittance windows in La-rich glasses correspond to those in B-rich glasses. Due to the fact that these two transmittance windows had large transmittance, the main absorption edge of La-rich glasses was taken as 1500 $\mathrm{cm^{-1}}$ (6.7 μm), which is much longer than that of B-rich glasses. It has been considered that borate glasses are not transparent in the near-IR (NIR) region. However, it was found that La-rich $\mathrm{La_2O_3}$–$\mathrm{B_2O_3}$ glasses had extra optical windows suitable for optical applications in the visible-to-NIR region.

Fig. 6 shows the refractive index dispersions of $x\mathrm{La_2O_3}$–(100 − x)$\mathrm{B_2O_3}$ glasses. It is clearly seen that the refractive index was increased by increasing the La content. The inset shows that the refractive index (n_d) at 587.56 nm increased linearly with x. A high refractive index, over 1.9, was achieved in La-rich glasses. Furthermore, it seems that the wavelength dispersion of La-rich glasses was small enough. Unfortunately, it is difficult to calculate the Abbe number of these glasses accurately, because the accuracy of the data obtained by the ellipsometer was not so high when the refractive index was less than 2.0. Nevertheless, the original goal, to increase the refractive

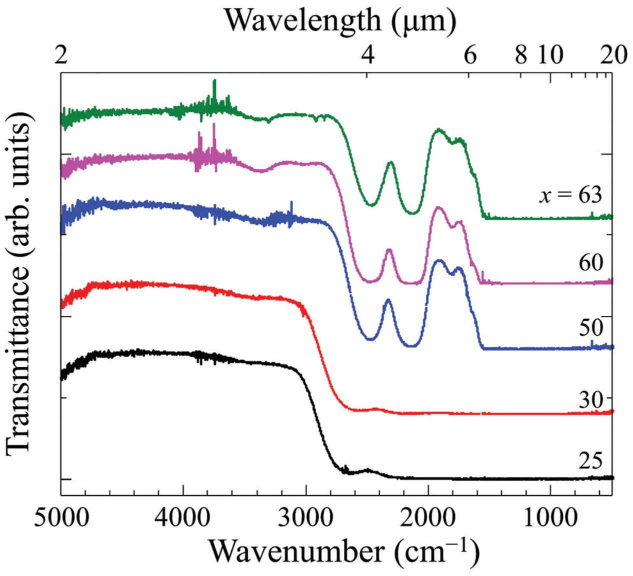

Fig. 5 IR transmittance spectra of $x\mathrm{La_2O_3}$–(100 − x)$\mathrm{B_2O_3}$ glasses.

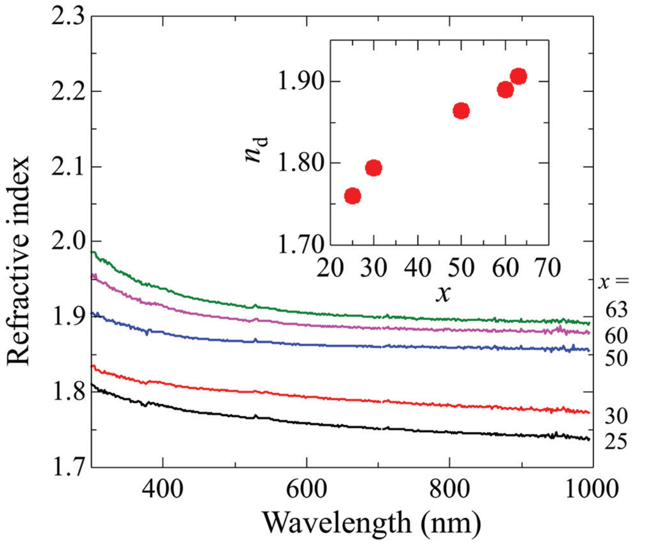

Fig. 6 Refractive index dispersions of $x\mathrm{La_2O_3}$–(100 − x)$\mathrm{B_2O_3}$ binary glasses. The inset shows the composition dependence of the refractive index at 571 nm (n_d).

index of low-wavelength-dispersion La_2O_3–B_2O_3 glasses by increasing the La_2O_3 content, was achieved.

Local structure around B

It is well known that the local structure around B-atoms in borate glasses undergoes complex changes of structural groups with the increase in modifier oxides.[31] In B_2O_3 glass, B- and O-atoms form boroxol ring networks where B-atoms are coordinated by three oxygen atoms. BO_4 units are formed *via* the addition of modifier oxides to B_2O_3 glasses. The fraction of BO_4 units to all BO_n units (n = 3 or 4) is called the N_4 value. This value increases when the content of the modifier oxides increases, before it reaches the maximum value at a certain amount of modifier oxides.[32] A further increase in the modifier oxides decreases the N_4 value. Generally, the results of NMR, Raman scattering, and IR spectra can be used to estimate N_4 values.[31–36]

Under a simple presumption that oxygen atoms introduced by modifier oxides are used to form BO_4 units without producing any nonbridging oxygen, N_4 can be easily estimated from chemical compositions. In the case of alkali borate glasses, x_AA_2O–$(100 - x_A)B_2O_3$, and alkali-earth borate glasses, x_MMO–$(100 - x_M)B_2O_3$, N_4 is calculated to be $X/(100 - X)$ ($X = x_A, x_M$). Experimentally obtained N_4 values agree rather well with the estimated data in the range $X < 30$, and they reach the maximum at approximately $X \sim 40$. This means that, at low concentrations of modifier oxides, $X < 30$, no nonbridging oxygen is formed in binary borate glasses as the simple presumption suggests. By further increasing X, networks of BO_3 and BO_4 units are broken and the number of structural units with nonbridging oxygen increases. There are few examples on local structure analyses around B-atoms at much larger X due to the low glass-forming ability over $X \sim 40$, although it was reported that N_4 certainly decreased with X and became almost zero at $X = 70$ in the case of alkali borate glasses.[31] This means that glass formation in borate systems requires network structures composed of BO_3 or BO_4 units.

In order to consider structural changes depending on the amount of modifier oxides in rare-earth borate glasses, xR_2O_3–$(100 - x)B_2O_3$, and to compare alkali borate and alkali-earth borate glasses, the chemical composition should be modified to $x_RR_{2/3}O$–$(100 - x_R)B_2O_3$. The value of x_R corresponds to x_A and x_M, and N_4 is calculated to be $X/(100 - X)$ ($X = x_R$). Here, there is a relationship between x and x_R, as shown below.

$$x_R = \frac{300x}{100 + 2x}$$

Accordingly, in the case of xLa_2O_3–$(100 - x)B_2O_3$ system, glass-forming regions ($20 \le x \le 35$ and $50 \le x \le 63$) were translated to be $42.9 \le x_R \le 61.8$ and $75 \le x_R \le 83.6$, respectively. Since the x_R value corresponding to even the smallest x of 20 was already as large as 42.9, N_4 should decrease by increasing x_R and reach zero, referring to the cases of alkali borate and alkali-earth borate glasses. B-rich glasses might still have BO_4 units. However, x_R in La-rich glasses is much larger than 70, indicating that La-rich glasses may not have any BO_4 units.

Fig. 7(a) shows the results of ^{11}B MAS NMR of xLa_2O_3–$(100 - x)B_2O_3$ glasses. The ^{11}B-atom has $I = 3/2$ nuclear spin. In addition, the NMR spectrum is affected by a second-order quadrupole interaction that depends on three parameters: isotropic chemical shift (δ_{iso}), quadrupole coupling constant (C_Q), and quadrupole asymmetry parameter (η). δ_{iso} reflects the degree of connectivity of BO_n units. C_Q is a function of electric field gradient at the nucleus eq and nuclear quadrupole moment eQ, which can be accordingly defined as $C_Q = e^2qQ/h$. C_Q is a measure of symmetry for a coordination shell around a

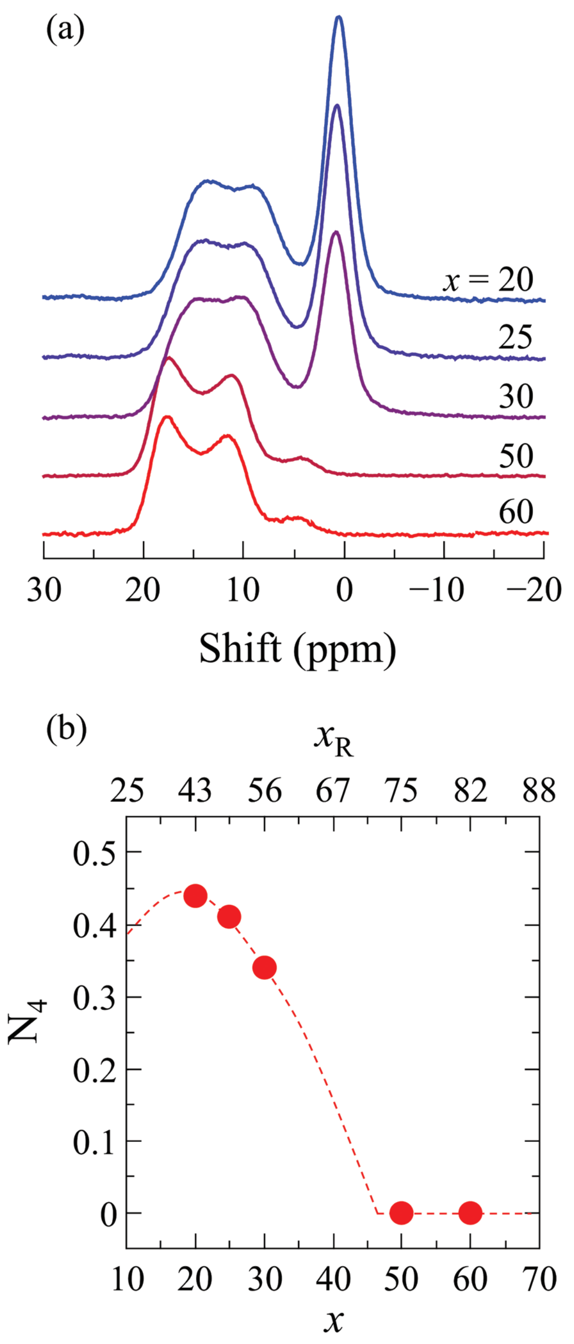

Fig. 7 (a) ^{11}B NMR spectra of xLa_2O_3–$(100 - x)B_2O_3$ binary glasses. (b) Composition dependence of N_4 values. The dashed line is a guideline.

nucleus. η describes the deviation of the electric field gradient from the axial symmetry.[37] The ^{11}B MAS NMR spectral decomposition for binary borate glasses is usually performed using one Gaussian/Lorentzian line for the BO_4 site and two quadrupolar lines including a Gaussian distribution on the chemical shift for BO_3 units.[38] The parameters δ_{iso}, C_Q, and η deduced from the fitting are shown in Table 1.

The sharp peak at approximately 0 ppm of δ_{iso}, which corresponds to BO_4 units, was clearly seen only in B-rich glasses. The relative peak intensity was decreased by increasing the La_2O_3 content, and it became zero in La-rich glasses. The fractions of BO_3 and BO_4 units were estimated using the integral of fitted curves and were used to calculate the N_4 value, as shown in Table 1. Fig. 7(b) shows the composition dependence of N_4 values, which agrees well with those of alkali borate and alkali-earth borate glasses considering the x_R value. Accordingly, the formation of BO_4 and BO_3 with non-bridging oxygen by the addition of modifier oxides can be discussed quantitatively and universally for alkali, alkali-earth, and rare-earth borate glasses.

Here, the details regarding the parameters for BO_4 and BO_3 peaks of the binary La_2O_3–B_2O_3 glasses were investigated. In the case of B-rich glasses, the observed shift of δ_{iso} for the BO_4 peak might be caused by the effect of BO_3 peaks, which even shifted to larger values from 0.5 to 0.83 by increasing the La_2O_3 content. The BO_4 sites had negligible second-order quadrupolar broadening with C_Q and η, indicating a high symmetrical environment around B-atoms.

The peak due to BO_3 units changed its shape and shifted to a large chemical shift in B-rich glasses, whereas the spectra of La-rich glasses were almost identical to each other in shape and position. The spectral change indicates the local structure change of BO_3 units. In order to discuss the local structure of the BO_3 unit using NMR parameters, the work reported by Kroeker and Stebbins is highly helpful.[39] They precisely examined the correlations between short-range structures around the BO_3 unit in various kinds of crystalline borate compounds and their chemical shift δ_{iso}. The values of δ_{iso} were clearly categorized by the bonding characteristics of trigonal BO_3 units, T^0, T^1, T^2-ring, T^2, T^3-ring, and T^3, where T and the superscripts mean the capital of trigonal and number of bridging oxygen atoms, respectively. It is indicated that δ_{iso} of BO_3 units in the range of around 10–25 ppm moved to the downfield region as the number of bridging oxygen atoms decreased, as in the inequality $\delta_{iso}(T^0) \geq \delta_{iso}(T^1) > \delta_{iso}(T^2\text{-ring}) > \delta_{iso}(T^2) \geq \delta_{iso}(T^3\text{-ring}) > \delta_{iso}(T^3)$. Kashiwakura *et al.* developed a two-dimensional map with δ_{iso} and η for a variety of T species.[40] The η values of BO_3 peaks were significantly small (<0.1) when the number of bridging oxygen atoms was zero or three, owing to the symmetrical electric field gradient around B-atoms. On the other hand, the η values of T^1 and T^2 became higher ($\geq$0.4) because of the asymmetrical coordination of the boron nucleus.

Table 1 ^{11}B NMR parameters, chemical shift (δ_{iso}), quadrupolar constant (C_Q), and asymmetry parameter (η), extracted from spectral decompositions using the Gaussian/Lorentzian and Q MAS 1/2 models for the B4 and B3 signals, respectively

Sites	δ_{iso} (ppm)	C_Q (MHz)	η	Fraction (%)	N_4
x = 20					0.44
BO_4	0.52	—	—	44	
BO_3 I	16.5	2.34	0.45	13	
BO_3 II	18.4	2.70	0.08	43	
x = 25					0.41
BO_4	0.73	—	—	42	
BO_3 I	17.4	2.34	0.4	21	
BO_3 II	19.3	2.79	0.08	37	
x = 30					0.34
BO_4	0.83	—	—	34	
BO_3 I	18.0	2.53	0.5	29	
BO_3 II	19.7	2.70	0.08	38	
x = 50					0
BO_4	—	—	—	0	
BO_3 I	—	—	—	0	
BO_3 II	21.3	2.67	0.08	100	
x = 60					0
BO_4	—	—	—	0	
BO_3 I	—	—	—	0	
BO_3 II	21.3	2.67	0.08	100	

These previous NMR data were acquired with an external magnetic field strength of 14.1 T, which is different from our experimental conditions. There may be a little concern about comparing our data with those ones. However, it was confirmed the differences in NMR parameters between 11.7 and 18.8 T are small enough.[41] Therefore, the classification mentioned above is available for this study. For the spectra of x = 20, 25, and 30 glasses, there were two BO_3 NMR signals referred to as BO_3 I and BO_3 II. δ_{iso} of BO_3 II is larger than that of BO_3 I. Two δ_{iso}'s shifted to high values by increasing the La_2O_3 content. η of BO_3 I was as large as 0.4–0.5, whereas that of BO_3 II was significantly small. BO_3 I was in the range between T^1 and T^2. By increasing the La_2O_3 content, BO_3 I shifted from the T^2 to the T^1 region.

For La-rich glasses, one BO_3 site is enough to fit the spectra. The large chemical shift of approximately 20 ppm and the small η correspond to T^0 values and are also almost the same values of orthoborate $LaBO_3$. Therefore, in La-rich glasses, there was no BO_4 as expected from the simple estimation using chemical composition. In addition, there was no bridged BO_3, but isolated BO_3.

The Raman scattering spectra of $x La_2O_3$–$(100 - x)B_2O_3$ glasses, as shown in Fig. 8, strongly support the composition dependence of the local structure around B and the existence of isolated BO_3 units as shown from the NMR results. In the B-rich region, the peak intensity of the spectra changed depending on the composition, whereas the shift was small. The band assignment for the spectra of B-rich glasses was carried out by referring alkali and alkali-earth borate binary glasses.[42,43] The bands of 659, 839, and 929 cm^{-1} correspond to the B–O–B stretching vibration of BO_3 units in depolymerized groups with only BO_3 triangles such as metaborate rings, pyroborate groups, and orthoborate groups, respectively. The band of 768 cm^{-1} is assigned to the vibration of the ladder-type ring unit ($2BO_3 + 2BO_4$ units) existing in the LaB_3O_6 crystalline structure. The band of 240 cm^{-1} is due to La–O bonds.

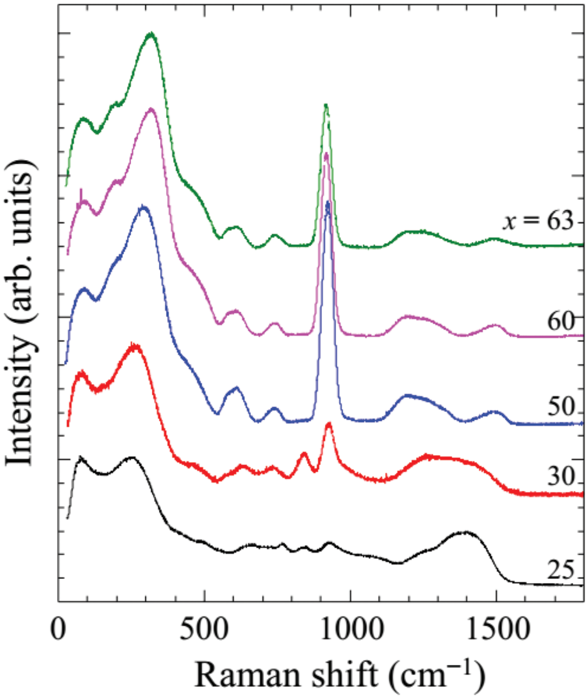

Fig. 8 Raman scattering spectra of $x\mathrm{La_2O_3}$–(100 − x)$\mathrm{B_2O_3}$ binary glasses.

At x = 30, the band from orthoborate shifted to a low wavenumber side of 920 $\mathrm{cm^{-1}}$, and the intensity was increased drastically. The band from pyroborate also shifted to a low wavenumber side and the intensity was slightly increased. These results agree with the composition dependence of N_4 values and NMR results, indicating the progress of fragmentation of the $\mathrm{BO_3}$ network by increasing the $\mathrm{La_2O_3}$ content.

By further increasing the La content, the spectra were almost identical to each other in La-rich glasses. In La-rich glasses, no peak shift and no intensity change were found. This means no change in the environment around B. There are intense bands at 602, 743, 917, 1190, and 1490 $\mathrm{cm^{-1}}$, which correspond to the reported values for crystalline $\mathrm{LaBO_3}$ of 585, 596, 621, 932, 1228, 1249, and 1369 $\mathrm{cm^{-1}}$.[44] This result indicates that the local structure around B-atoms of La-rich glasses resembled that of crystalline $\mathrm{LaBO_3}$. There is one B-site in crystalline $\mathrm{LaBO_3}$. A B-atom is coordinated to three oxygen atoms, and the $\mathrm{BO_3}$ units are isolated. The trigonal planar $\mathrm{BO_3}$ units form an infinite net that lies perpendicular to the c-axis, with $\mathrm{La^{3+}}$ ions residing between the layers. Each $\mathrm{La^{3+}}$ is coordinated to nine oxygen atoms from six different borates.

From the results of NMR and Raman scattering spectra, it is concluded that La-rich glasses had only isolated $\mathrm{BO_3}$ units, meaning a simple environment around B-atoms. The effect of the disappearance of a variety of BO_n units on the physical properties was seen in the IR spectra in Fig. 5. In the IR transmittance spectra at the B-rich composition, the absorption edge was approximately 2700 $\mathrm{cm^{-1}}$. IR light below the energy was absorbed by multiple vibrations of various types of BO_n units. On the other hand, the absorption edge was 1500 $\mathrm{cm^{-1}}$ in the La-rich composition, even though there were some absorption peaks between 2700 and 1500 $\mathrm{cm^{-1}}$. The IR transmittance spectra of La-rich glasses are similar to those of crystalline $\mathrm{LaBO_3}$.[45] The remnant absorption, thus, was caused by B–O vibration only in isolated $\mathrm{BO_3}$ triangles. Therefore, the small value of the absorption edge of La-rich glasses was due to the absence of a variety of BO_n units, which caused large absorption in a wide region. Although binary borate glass systems are conventional in glass science, the simplification of the local structure around B-atoms caused the wide transmittance in the IR region. The La-rich glasses are suitable materials from UV to NIR regions with a high refractive index and low wavelength dispersion. Very recently, Tb-rich borate glasses with a large Faraday effect have been developed by a levitation technique.[46] These results indicate that there is still a possibility of adding further functionalities to conventional glass systems by extending glass-forming regions and tuning local structures.

Conclusion

$x\mathrm{La_2O_3}$–(100 − x)$\mathrm{B_2O_3}$ glasses were fabricated *via* containerless processing using an aerodynamic levitation technique. In addition to the expansion of the glass-forming region in the B-rich composition, a new glass-forming region was discovered in La-rich regions. All of these glasses were colorless and transparent in the visible region. The absorption edge shifted to a long wavelength by increasing the La content. The refractive index increased monotonically by increasing the La content, and these glasses showed very low wavelength dispersion. The local structure around B-atoms was investigated. In La-rich glasses, completely isolated B-atoms were found. The few kinds of BO_n units decreased the multiphonon process and then new transmittance windows were obtained in the NIR region.

Conflicts of interest

There are no conflicts to declare.

Acknowledgements

This study was supported in part by Chemical Innovation Encouragement Prize, the Collaborative Research Project of Materials and Structures Laboratory, Tokyo Institute of Technology, the Collaborative Research Program of Institute for Chemical Research, Kyoto University, "Materials research by Information Integration" Initiative ($\mathrm{MI^2I}$) project of the Support Program for Starting Up Innovation Hub from Japan Science and Technology Agency (JST), and JSPS KAKENHI (Grant numbers JP25410236, JP26249092, JP17H03121, and JP18K18928).

References

1 D. L. Price, *High-Temperature Levitated Materials*, Cambridge University Press, 2010.

2 D. Herlach, D. Holland-Moritz and P. Galenko, *Metastable Solids from Undercooled Melts*, Elsevier, 2007.

3 S. Kohara, K. Suzuya, K. Takeuchi, C. K. Loong, M. Grimsditch, J. K. R. Weber, J. A. Tangeman and T. S. Key, *Science*, 2004, **303**, 1649–1652.

4 G. A. Rosales-Sosa, A. Masuno, Y. Higo and H. Inoue, *Sci. Rep.*, 2016, **6**, 23620.

5 J. K. R. Weber, J. J. Felten, B. Cho and P. C. Nordine, *Nature*, 1998, **393**, 769–771.

6 J. Yu, Y. Arai, T. Masaki, T. Ishikawa, S. Yoda, S. Kohara, H. Taniguchi, M. Itoh and Y. Kuroiwa, *Chem. Mater.*, 2006, **18**, 2169–2173.

7 A. Masuno and H. Inoue, *Appl. Phys. Express*, 2010, **3**, 102601.

8 K. Yoshimoto, A. Masuno, H. Inoue and Y. Watanabe, *J. Am. Ceram. Soc.*, 2012, **95**, 3501–3504.

9 G. A. Rosales-Sosa, A. Masuno, Y. Higo, H. Inoue, Y. Yanaba, T. Mizoguchi, T. Umada, K. Okamura, K. Kato and Y. Watanabe, *Sci. Rep.*, 2015, **5**, 15233.

10 P. Kidkhunthod, A. Bootchanont and A. C. Barnes, *J. Non-Cryst. Solids*, 2016, **448**, 27–30.

11 A. Masuno, H. Inoue, J. Yu and Y. Arai, *J. Appl. Phys.*, 2010, **108**, 063520.

12 A. Masuno, H. Inoue, K. Yoshimoto and Y. Watanabe, *Opt. Mater. Express*, 2014, **4**, 710.

13 K. Yoshimoto, A. Masuno, M. Ueda, H. Inoue, H. Yamamoto and T. Kawashima, *Sci. Rep.*, 2017, **7**, 45600.

14 H. Inoue, Y. Watanabe, A. Masuno, M. Kaneko and J. Yu, *Opt. Mater.*, 2011, **33**, 1853–1857.

15 A. Masuno, Y. Watanabe, H. Inoue, Y. Arai, J. Yu and M. Kaneko, *Phys. Status Solidi C*, 2012, **9**, 2424–2427.

16 K. Yoshimoto, A. Masuno, H. Inoue and Y. Watanabe, *J. Am. Ceram. Soc.*, 2015, **98**, 402–407.

17 K. Yoshimoto, A. Masuno, M. Ueda, H. Inoue, H. Yamamoto and T. Kawashima, *J. Am. Ceram. Soc.*, 2018, **101**, 3328–3336.

18 H. Bach and N. Neuroth, *The Properties of Optical Glasses*, Springer, 1995.

19 S. Tomeno, J. Sasai and Y. Kondo, *Phys. Chem. Glasses*, 2009, **50**, 172–174.

20 I. N. Chakraborty, J. E. Shelby and R. A. Condrate, *J. Am. Ceram. Soc.*, 1984, **67**, 782–785.

21 E. M. Levin, C. R. Robbins and J. L. Waring, *J. Am. Ceram. Soc.*, 1961, **44**, 87–91.

22 M. Imaoka and T. Yamazaki, *J. Ceram. Assoc. Jpn.*, 1962, **70**, 89–100.

23 O. V. Mazurin, M. V. Streltsina and T. P. Shvaiko-Shvaikovskaya, *Handbook of Glass Data Part B single-component and binary non-silicate oxide glasses*, Elsevier, NY, 1985.

24 K. Terashima, S. Tamura, S.-H. Kim and T. Yoko, *J. Am. Ceram. Soc.*, 1997, **80**, 2903–2909.

25 A. C. Vaz de Araújo, I. T. Weber, B. S. Santos, B. J. P. da Silva, R. P. de Mello Jr., S. Alves Jr., G. F. de Sá and C. de Mello Donegá, *J. Non-Cryst. Solids*, 1997, **219**, 160–164.

26 A. Kajinami, M. Nakamura and S. Deki, *J. Alloys Compd.*, 2006, **408–412**, 1238–1241.

27 D. S. Pytalev, D. Caurant, O. Majérus, H. Trégouët, T. Charpentier and B. N. Mavrin, *J. Alloys Compd.*, 2015, **641**, 43–55.

28 D. Massiot, F. Fayon, M. Capron, I. King, S. Le Calvé, B. Alonso, J. O. Durand, B. Bujoli, Z. Gan and G. Hoatson, *Magn. Reson. Chem.*, 2002, **40**, 70–76.

29 R. Ohta and N. Soga, *Yogyo Kyokaishi*, 1982, **90**, 531–537.

30 A. Masuno, S. Kohara, A. C. Hannon, E. Bychkov and H. Inoue, *Chem. Mater.*, 2013, **25**, 3056–3061.

31 E. I. Kamitsos and M. A. Karakassides, *Phys. Chem. Glasses*, 1989, **30**, 19–26.

32 J. Zhong and P. J. Bray, *J. Non-Cryst. Solids*, 1989, **111**, 67–76.

33 E. I. Kamitsos and G. D. Chryssikos, *J. Mol. Struct.*, 1991, **247**, 1–16.

34 B. N. Meera and J. Ramakrishna, *J. Non-Cryst. Solids*, 1993, **159**, 1–21.

35 Y. D. Yiannopoulos, G. D. Chryssikos and E. I. Kamitsos, *Phys. Chem. Glasses*, 2001, **42**, 164–172.

36 J. Wu and J. F. Stebbins, *J. Am. Ceram. Soc.*, 2014, **97**, 2794–2801.

37 K. J. D. Mackenzie and M. E. Smith, *Multinuclear Solid-State NMR of Inorganic Materials*, Pergamon, 2002.

38 J. D. Epping, H. Eckert, A. W. Imre and H. Mehrer, *J. Non-Cryst. Solids*, 2005, **351**, 3521–3529.

39 S. Kroeker and J. F. Stebbins, *Inorg. Chem.*, 2001, **40**, 6239–6246.

40 S. Kashiwakura, T. Takahashi, H. Maekawa and T. Nagasaka, *Fuel*, 2010, **89**, 1006–1011.

41 F. Angeli, T. Charpentier, D. de Ligny and C. Cailleteau, *J. Am. Ceram. Soc.*, 2010, **93**, 2693–2704.

42 N. P. Lower, J. L. McRae, H. a. Feller, A. R. Betzen, S. Kapoor, M. Affatigato and S. a. Feller, *J. Non-Cryst. Solids*, 2001, **293–295**, 669–675.

43 R. Brow, D. Tallant and G. Turner, *J. Am. Ceram. Soc.*, 1996, **79**, 2410–2416.

44 H. Giesber, J. Ballato, G. Chumanov, J. Kolis and M. Dejneka, *J. Appl. Phys.*, 2003, **93**, 8987–8994.

45 M. Tukia, J. Hölsä, M. Lastusaari and J. Niittykoski, *Opt. Mater.*, 2005, **27**, 1516–1522.

46 F. Suzuki, F. Sato, H. Oshita, S. Yao, Y. Nakatsuka and K. Tanaka, *Opt. Mater.*, 2018, **76**, 174.